Role played by the coupling effects in the elastic scattering of ^{6}He on ^{12}C

V. Lapoux* and N. Alamanos, F. Auger, V. Fékou-Youmbi,
A. Gillibert, F. Marie, S. Ottini-Hustache, J-L. Sida
CEA-SACLAY DSM/DAPNIA/SPhN F-91191 Gif-sur-Yvette, France.

D.T. Khoa
Institute for Nuclear Science and Technique, VAEC,
P.O. Box 5T-160, Nghia Do, Hanoi, Vietnam.

Y. Blumenfeld, F. Maréchal,† J-A. Scarpaci, T. Suomijärvi, and J.H. Kelley‡
Institut de Physique Nucléaire, IN_2P_3-CNRS, F- 91406 Orsay, France.

J-M. Casandjian, M. Chartier,§ M.D Cortina-Gil,¶ M. Mac Cormick,** W. Mittig, F. de Oliveira Santos, A.N. Ostrowski,†† and P. Roussel-Chomaz
GANIL, Bld Henri Becquerel, BP 5027, 14021 Caen Cedex, France.

K. W. Kemper
Department of Physics, Florida State University, Tallahassee, Fl 32306, USA.

N. Orr and J.S. Winfield‡‡
LPC-ISMRA, Bld du Maréchal Juin, 14050 Caen Cedex, France

(Dated: August 30, 2002)

Abstract

To study the effect of the weak binding energy on the interaction potential between a light exotic nucleus and a target, elastic scattering of ^{6}He at 38.3 MeV/nucleon on ^{12}C target was measured at GANIL. The ^{6}He beam was produced by fragmentation. The detection of the scattered particles was performed by the GANIL spectrometer. The energy resolution was good enough to separate elastic from inelastic scattering contributions. The measured elastic data have been analyzed within the optical model, with the real part of the optical potential calculated in the double-folding model using a realistic density dependent nucleon-nucleon interaction and the imaginary part taken in the conventional Woods-Saxon (WS) form. A failure of the 'bare' real folded potential to reproduce the measured angular distribution over the whole angular range suggests quite a strong coupling of the higher-order breakup channels to the elastic channel. To estimate the strength of the breakup effects, a complex surface potential with a *repulsive* real part (designed to simulate the polarization effects caused by the projectile breakup) was added to the real folded and imaginary WS potentials. Realistic estimate of the polarization potential caused by the breakup of the weakly bound ^{6}He was made based on a parallel study of ^{6}He+^{12}C and ^{6}Li+^{12}C optical potentials at about the same energies.

PACS numbers: 21.30.Fe, 24.10.-i, 25.60.Bx, 25.60.-t, 27.20.+n

*E-mail : vlapoux@cea.fr; URL: http://www-dapnia.cea.fr/Sphn/Exotiques

†permanent address : IReS BP 28 F-67037 Strasbourg, France.

‡present address : Department of Physics, North Carolina State University Raleigh, North Carolina, 27695.

§present address : Department of Physics, University of Liverpool, Liverpool L69 7ZE UK.

¶permanent address : Facultad de Fisica, Dpto de particulas, Santiago de Compostela 15706 Spain.

**permanent address : IPN, IN2P3 F- 91406 Orsay, France.

††permanent address : Department of Physics & Astronomy, University of Edinburgh, Edinburgh, EH9 3JZ UK.

‡‡present address : INFN - Laboratori Nazionali del Sud, Via Sofia 44, Catania, Italy.

I. INTRODUCTION

Radioactive beams have been developed worldwide for the last twenty years, offering the possibility to explore new phenomena in the nuclear matter, at the limits of the nuclear stability [1]. The study of the light neutron-rich nuclei has revealed a new class of exotic nuclei which are abnormally extended [2]. Among these nuclei, those qualified as halo nuclei [3] such as ^{6}He and ^{11}Li, require special treatments of their structural and dynamic properties which take into account their few-body correlations.

The neutron-halo nucleus ^{6}He appears as one of the best examples of a nuclear three-body system : it can be easily described as a tightly bound α-core plus two valence neutrons, with the two-neutron separation energy (2n+α) of 0.975 MeV [4, 5]. It is also qualified as a borromean nucleus because none of its binary subsystems is bound. The wave functions of the valence neutrons forming the "halo" have a large spatial extension, with respect to the range of strong interaction. The halo itself is a direct consequence of the weak binding of the valence nucleons that allows the wave functions to tunnel out of the core potential.

Experimentally, the structure of the ^{6}He was investigated through the measurement of interaction cross sections and cross sections for the inelastic scattering and neutron knock-out by a carbon target at energy of 790 MeV/nucleon [2, 6]. Proton elastic scattering of ^{6}He beams was measured at 717 MeV/nucleon at GSI [7], at 70 MeV/nucleon at Riken [8], at 38.3 MeV/nucleon at Ganil [9], and at 25 MeV/nucleon at Dubna [10]. The low-lying excitations in ^{6}He have also been investigated [11, 12]. Theoretically, ^{6}He has been investigated in the framework of numerous three-body calculations [5, 13–15], as well as in the variational quantum Monte Carlo shell model approach [16], using the two-body and three-body nucleon-nucleon interactions. All these models describe rather well the structure of ^{6}He, like the binding energy and the nuclear density distribution [17], and confirm a consistent halo picture for ^{6}He nucleus. The features of the ground state density distribution, and a ^{6}He root mean square (rms) matter radius of the order of 2.54 ± 0.04 fm were deduced from the few-body analysis of the elastic scattering [17] or reaction cross sections [18].

The striking feature of the halo nuclei is the long tail of their matter density, due to their weak binding energy. The weak binding also implies that they can easily decay to cluster states. In fact, their particle threshold found to be close to their ground state should imply a strong coupling to the continuum during the interaction of a halo nucleus with

a target. All this requires a special treatment of the interaction potential between a *halo* projectile and a *stable* target. In general, one must take into account explicitly the couplings to the transitions to the low-lying excited states as well as to the resonance and breakup states (continuum) [19]. Such couplings give rise to the so-called dynamic polarization potential (DPP) that should be added to the microscopic optical potential. However, an accurate calculation of the DPP is rather complicated and requires a detailed knowledge of the spectroscopic structure of the two colliding nuclei [20, 21]. Besides the breakup into the 2n+α channel, other complicated processes involving the core breakup can also contribute to the DPP. For example, the core break-up in ^{6}He has been described using an extended microscopic α+n+n cluster model [22] and it has been found that the core breakup effect can lead to the t+t channel. All such channels are important and should be included into a coupled reaction channel model for a correct description of the elastic ^{6}He scattering.

Within the standard optical model (OM), the double-folding approach has been used earlier [23] to generate the 'bare' nucleus-nucleus part of the real optical potential for ^{11}Li+^{12}C system. Higher-order contributions of the DPP (due to the breakup) have been added in a phenomenological way, to provide a qualitative understanding of the role of the breakup effects in the elastic scattering of the *halo* ^{11}Li nucleus. At GANIL (Grand Accélérateur NAtional d'Ions Lourds, Caen, France), we have measured angular distributions of elastic scattering of the radioactive ^{6}He beam on ^{12}C at the energy of 38.3 MeV/nucleon.

Our first aim, in measuring elastic scattering data for ^{6}He, was to determine whether the optical potentials, obtained through folding model calculations and using the effective NN interactions, already proven to be well adapted to the stable nuclei, with the notable exception of the ^{6}Li and ^{9}Be [24], were still valid in the case of light exotic nuclei. As a second step of our study, we will estimate the effect caused by the projectile breakup following a similar approach as described in Ref. [23], and check whether the weak binding of the light exotic nucleus ^{6}He should appreciably enhance the polarization potential, which simulates all the break-up effects. In Ref. [9], a similar study was performed, but for the analysis of elastic data for ^{6}He on proton target at the same energy, 38.3 MeV/nucleon. A microscopic nucleus-nucleon potential was used, and it was shown that the couplings to the continuum play an important role in the proton elastic scattering of the ^{6}He at energies below 100 MeV/nucleon.

The good energy resolution of the energy-loss spectrometer SPEG render the present data

free of contamination by inelastic scattering on the excited states of the target. It is then possible to study unambiguously the interaction potential between the light exotic nucleus ^{6}He and the carbon target and as well to investigate the effect of the weak binding energy on the elastic scattering data.

In a previous experiment at GANIL, reported in Ref. [25], elastic data for the ^{6}He + ^{12}C did not extend to large enough angles to draw conclusions about the ^{6}He + ^{12}C optical potential. Previous results concerning exotic nuclei, for instance, ^{11}Li + ^{12}C [26], were in fact quasi-elastic measurements : the energy resolution of the detectors did not resolve the elastic and inelastic scattering contributions. In the experiment presented here, the purely elastic data were measured with a better angular resolution and over a larger angular range.

We show in this article that these new ^{6}He+^{12}C data can be well reproduced and interpreted within the framework of the double folding model, taking into account new effective NN interactions [27] and a simple form for the polarization potential. The comparison between the interaction potential for both systems ^{6}He-^{12}C and α-^{12}C gives insights on the role played by the halo in the elastic scattering.

In Section II the experimental set-up is described. In Section III, the folding model has been applied to the analysis of data from elastic scattering of alpha-particles on a carbon target at different energies, in order to obtain a coherent description of the α-^{12}C potential at 38.3 MeV/nucleon. Then, a first analysis of the ^{6}He-^{12}C data is performed in Section IV by using a phenomenological polarization potential. In Section V we present the analysis of the ^{6}Li on ^{12}C with a new density-dependent interaction, CDM3Y6. ^{6}Li is also an $A = 6$ system with a loosely bound structure. The total potential (including the polarization potential) for ^{6}Li+^{12}C is deduced and helps in better defining the polarization potential of the ^{6}He +^{12}C system. The optical potential for ^{6}He on ^{12}C is discussed and the effect of the break-up process on the elastic scattering of the ^{6}He-^{12}C system is investigated. Conclusions on the role of the polarization potential in the elastic scattering of weakly bound projectiles are drawn in Sec. VI.

II. EXPERIMENTAL SET-UP AT GANIL

Elastic angular cross sections of ^{6}He on a 10 mg/cm^2 thick polypropylene target $(CH_2CHCH_3)_n$ (density of 0.896 g/cm^3) were measured at GANIL with the high resolution

energy-loss spectrometer SPEG [28].

The ^{6}He secondary beam was produced by fragmentation of a 75 MeV/nucleon primary ^{13}C beam, delivered by the two GANIL cyclotrons, on a carbon production target located between the two superconducting solenoids of the SISSI device (Superconducting Intense Source for Secondary Ions) [29, 30]. This device is located at the exit of the second cyclotron and at the entrance of the beam analysing α-spectrometer, which allows for an improved collection of secondary beams and transmission to the different experimental areas. A degrader was put in the α-spectrometer in order to purify the secondary beam. After purification, the ^{6}He beam represented around 75 % of the total secondary beam. The intensity of the ^{6}He secondary beam on the reaction target in the SPEG area was of the order of 10^{5} pps at an energy of 38.3 MeV/nucleon.

The scattered particles were identified in the focal plane of the SPEG spectrometer by the energy loss measured in an ionization chamber and the residual energy measured in plastic scintillators. The momentum and the scattering angle after the target were obtained by track reconstruction of the trajectory as determined by two drift chambers located near the focal plane of the spectrometer. As is usual with exotic beams produced by the fragmentation method, the beam emittance was large, and the angular spread was of the order of 1 deg. So the incident angle of the beam on the target is required for the calculation of the scattering angle. The position and angle of the projectile on the target were determined event by event using two beam detectors located upstream of the target. These detectors are low pressure drift chambers mounted on profilers near the focal (object) point of the analysing dipole. Each one is a double X,Y position-sensitive detector with a 70 mm drift region corresponding to 1.4 μs maximum drift time. A full description of these detectors and of their multi-hit readout can be found in Ref. [31].

A position sensitive microchannel plate was placed in front of the target and provided the stop signal for the beam detectors. Fig. 1 shows two two-dimensional spectra measured in the focal plane of SPEG for the scattering of ^{6}He on the polypropylene target. The scattering angle (in the laboratory frame) is presented as a function of the energy loss. They are realized from the same sets of data, but using two different calculations for the scattering angle : the information corresponding to the incident angle given by the beam detectors is taken into account in the spectrum to the right, it is not the case in the other one on the left, for which the beam was assumed to be perpendicular to the target. This

latter assumption is used for stable beams, whose angular emittance on the target is small. The straight line to the right of each spectrum corresponds to the elastic scattering on ^{12}C, whereas the other line corresponds to inelastic scattering (^{6}He on ^{12}C*, the first excited state (2^{+}) of the ^{12}C is at 4.44 MeV). The broad curve corresponds to the elastic scattering on protons. Strong inverse kinematics and the large angular opening of the incident beam broaden the curve but, due to the measurement of the incident angle, this line is straightened on the right-hand spectrum, and the angular resolution is improved.
The energy resolution $\frac{\Delta E}{E} = 10^{-3}$ allows the measurement of elastic scattering angular distributions of light nuclei, with complete separation of inelastic scattering from target excitations. The angular resolution is 0.3° in the laboratory system. The ratio of angular distributions of differential cross sections to the Rutherford cross sections $\frac{d\sigma}{d\sigma_R}$ is plotted in Fig. 2 with the angle $\Theta_{c.m.}$ in the center of mass (c.m.) frame. The binning of the data corresponds to the angular resolution of the measurement, given in the center of mass frame : from 0.45 for the smaller angles (around 2° c.m.) to 0.75 at 19.9° c.m.

The first maximum around 4° c.m. is dominated by the Coulomb interaction and the calculated cross sections are almost insensitive to the nuclear potential used for the calculations of the elastic scattering. So all calculated cross sections for the system give the same first maximum and this provides the absolute normalization of the data. Systematic errors (on the normalization of the cross sections, and on the angle of the beam, which is monitored by the beam detectors) are negligible compared to the statistical errors, given by the error bars on the plot. Including all the systematic uncertainties (on the target thickness, on the monitoring of the incident beam by the beam detectors, on the acceptance of the detection system) the absolute normalization of the experimental data has a total systematic error of 14 %. We have checked that the experimental normalization of the data corresponds to the one given by the theoretical calculations at forward angles. Since the systematical error of the theoretical normalization gave a systematical error smaller than in the case of the experimental normalization (and smaller than the statistical errors) we have adopted it in the article. The systematic error on the scattering angle was evaluated to be 0.1° in the lab. system (0.15° c.m.) by comparing the experimental kinematics for the reactions of ^{6}He on ^{12}C and protons to the calculated ones, at 38.3 MeV/nucleon. Three maxima can be seen in Fig. 2. The $\frac{d\sigma}{d\sigma_R}$ cross sections increase with the angle, which is a behavior usually qualified as refractive. This trend is similar to the one observed in the elastic scattering

of alpha-particles on ^{12}C, ^{58}Ni, ^{70}Zn targets for energies from 100 MeV to 200 MeV [27]. A decomposition of the scattering amplitude between near and far-side components shows that the cross sections at larger angles are dominated by the far-side component, which is indicative of a strong refractive pattern [27]. One of the most fascinating features of the refractive scattering is that one can probe the interaction potential between the two nuclei at different distances, provided the data were accurately measured over a large angular range.

III. FOLDING MODEL ANALYSIS

It is well established that elastic α scattering on light and medium mass targets is strongly refractive at intermediate energies. In this case, the absorption is quite weak and the measured elastic cross sections were shown to be sensitive to the *real* optical potential not only at the surface but also at shorter distances. The real part V of the optical potential can be obtained microscopically in the folding model [24, 32], using the realistic effective NN interaction and matter (ground state) density distributions of the projectile and target. In this case, the refractive α-nucleus elastic scattering data can be very helpful in testing different models for the target density [32]. Given the success of the folding model in the OM analysis of the elastic α scattering, we choose to use this simple model in the present paper to calculate the (real) ^{6}He+^{12}C optical potentials for the OM analysis of the newly measured elastic ^{6}He+^{12}C data.

In the folding model, the projectile-target optical potential can be evaluated as a Hartree-Fock-type potential of the dinuclear system

$$U_F = \sum_{i\in P, j\in T} [< ij|v_D|ij > + < ij|v_{EX}|ji >] = V_D(E, \boldsymbol{R}) + V_{EX}(E, \boldsymbol{R}, \boldsymbol{R'}). \qquad (1)$$

where the nuclear interaction U_F is a sum of the effective NN interactions v_{ij} between nucleon i in the projectile P and the target T. The direct term is local (provided that the NN interaction itself is local), and can be written in terms of the one-body spatial densities,

$$V_D(E, \boldsymbol{R}) = \int \rho_P(\boldsymbol{r}_P)\rho_T(\boldsymbol{r}_T)v_D(\rho, E, s)d^3r_P d^3r_T, \qquad \boldsymbol{s} = \boldsymbol{r}_T - \boldsymbol{r}_P + \boldsymbol{R}, \qquad (2)$$

where $\rho_P(\boldsymbol{r}_P) \equiv \rho_P(\boldsymbol{r}_P, \boldsymbol{r}_P)$ is the diagonal part of the nonlocal (one-body) density matrix for the projectile, and similarly for $\rho_T(\boldsymbol{r}_T)$ for the target nucleus.

The exchange term is, in general, nonlocal. However, an accurate local approximation can be obtained by treating the relative motion locally as a plane wave [33] :

$$V_{EX}(E,\boldsymbol{R}) = \int \rho_P(\boldsymbol{r}_P, \boldsymbol{r}_P + \boldsymbol{s})\rho_T(\boldsymbol{r}_T, \boldsymbol{r}_T - \boldsymbol{s}) v_{EX}(\rho, E, s) \exp\left(\frac{i\boldsymbol{K}(E,\boldsymbol{R})\boldsymbol{s}}{M}\right) d^3r_P d^3r_T. \tag{3}$$

$\boldsymbol{K}(E,\boldsymbol{R})$ is the local momentum of relative motion determined as

$$K^2(E,\boldsymbol{R}) = \frac{2\mu}{\hbar^2}[E_{\text{c.m.}} - U_F(E,\boldsymbol{R}) - V_C(\boldsymbol{R})], \tag{4}$$

μ is the reduced mass, $M = A_p.A_t/(A_p + A_t)$ with A_p and A_t the mass numbers of the projectile and target, respectively. For further details of the new version of the folding model we refer the readers to Ref. [32] and references therein.

Since the G-matrix interaction [34] is real, the real folded potential $U_F(R)$ must be supplemented by an imaginary potential, usually seen as an absorptive volume potential caused by the loss of incident flux into non-elastic channels. While a microscopic evaluation of the imaginary potential is possible in principle (see for instance [35]) it is complicated for the case of the scattering of two composite nuclei. Moreover, it was shown from the analyses of refractive heavy ion scattering [21, 36] and from α-nucleus scattering [37] that the imaginary potential cannot be taken with the same shape as the real folded potential, due to the weak absorption of these systems. So the imaginary potential is phenomenological in this kind of analysis, and is taken as a standard Wood-Saxon (WS) form :

$$W(R) = -\frac{W_v}{1 + \exp\left((R - R_w)/a_w\right)}. \tag{5}$$

The total local optical potential $U(R)$ is written :

$$U(R) = V_C(R) + N_r U_F(R) + iW(R), \tag{6}$$

with U_F, the folding potential, N_r the normalization factor of the real potential, and W the imaginary part. The depth W_v, the radius R_w, the diffuseness a_w and the normalization N_r can be adjusted in order to reproduce the data [38].

To compare results obtained for different scattering systems, it is also convenient to use the reduced radius r_w which is defined as $r_w = R_w/(A_p^{1/3.} + A_t^{1/3.})$. The Coulomb potential in our analysis is taken as the usual Coulomb form between a point charge and a uniform charge distribution of the radius $R_c = r_c(A_t^{1/3} + A_p^{1/3})$ with r_c =1.2 fm.

The calculations of cross sections and all the OM analyses are performed using the ECIS (Sequential Iteration of Coupled-Channel Equations) code written by Raynal [39]. The projectile matter distribution, in the case of unstable projectiles, is obtained from microscopic calculations. The target density is deduced from the charge distribution obtained by electron scattering measurements.

For the choice of the analytical density and energy-dependent form for the interaction V_{NN} included in Eqs. 2 and 3, we examine here the recently parametrized density dependent versions of the M3Y interaction [27, 40] based on the G-matrix elements of the Paris NN interaction [34]. It is written as a combination of the direct (V_D) and exchange (V_{EX}) parts :

$$\begin{aligned} V_{D(EX)}(r,\rho,E) &= V_{D(EX)}^{M3Y}(r) \times \mathcal{F}(\rho) g(E) \\ &= V_{D(EX)}^{M3Y}(r) \times \mathcal{F}(\rho)[1 - G\frac{E}{A}] \end{aligned} \tag{7}$$

All the interactions BDM3Y1, CDM3Yn, n=1,6 described in Ref. [27] have the general form of Eq. 7. E/A is the energy per nucleon and ρ the density of the two overlapping nuclei, defined as being the sum of the densities of their ground states, evaluated at the midpoint of the internucleon separation. The interaction is combined, as in the case of DDM3Y, to the $V_{D(EX)}^{M3Y}$ term which is here the Paris interaction, with its exchange term (EX) treated explicitly, as explained in Ref [41] and as seen above (Eq. 3). The authors of Ref. [40] required, to simplify, that the parameters of the density-dependent part $\mathcal{F}$ of the interaction be independent of the energy. All the energy dependence is included in the function $g(E)$. A parametrization of the effective interaction was searched in [40], which satisfies both the properties of saturation of the nuclear matter as well as the empirical energy-dependence of the nucleon nucleon potential. In the case of the Paris-version of the V^{M3Y} term, G is equal to 0.003 MeV^{-1}. A power-law density dependence was associated with the original Paris-M3Y interaction V^{M3Y} to create BDM3Y1(Paris), so its density function is written $\mathcal{F} = C(1 - \alpha\rho^{\beta})$, where $C = 1.2521$, α=1.7452 fm^3 and $\beta = 1$. The density dependence $\mathcal{F}(\rho)$ of CDM3Y6 is a hybrid form between DDM3Y1 (see [40]) and BDM3Y1 : $\mathcal{F}(\rho) = C[1 + \alpha e^{-\beta\rho} - \gamma\rho]$.

Its parameters are : $\alpha = 3.8033$, $\beta = 1.4099$ fm^3, $\gamma = 4.0$ fm^3 and $C = 0.2658$. Note that the values for the nuclear matter incompressibility are $K = 252$ MeV and 270 MeV for CDM3Y6 and BDM3Y1 interactions, respectively. These new energy and density-dependent effective

NN interactions, BDM3Y1 and CDM3Y6, were developed and applied successfully [27] to nucleus-nucleus systems for which the elastic scattering presents strong refractive patterns, as for instance, in the case of α + nucleus. The interaction of the exotic nucleus ^{6}He with ^{12}C will be described here by using these two NN interactions.

A. First analysis of the ^{6}He + ^{12}C elastic scattering

We calculate the real part of the interaction potential, U_F, with the folding model which includes the effective interaction NN BDM3Y1 (Paris) or CDM3Y6 [27], folded with the matter density of the ^{6}He particle and with the carbon one. The ground state matter density of ^{12}C is taken as a two-parameter Fermi function, with $\rho_o = 0.207$ fm^{-3}, $C_p = 2.1545$ fm and $a_p = 0.425$ fm ; these parameters were adjusted in Ref. [42] to have a rms radius of 2.298 fm close to those obtained from (e, e) scattering measurements. This density has a similar shape as the one obtained by shell model calculations [42].

To study the effect caused by the halo structure of ^{6}He, various versions of the ground state density distribution have been used in the folding calculation. We have used a halo-type density for the ^{6}He, obtained by three-body model calculations [43]. This density, denoted as *fc6*, corresponds to the correct binding energy (with the two-neutron separation energy S_{2n} of 0.97 MeV). The matter rms radius of the *fc6* density is equal to 2.54 fm, close to the value evaluated from the four-body analysis of the ^{6}He+ ^{12}C total reaction cross sections [43], and by the analysis of elastic scattering of ^{6}He on proton at high energies [17]. Implicitly, the *fc6* density includes 3-body correlations. To characterize all the break-up effects that should be included in the total interaction potential, a compact gaussian density is also used instead of the *fc6* density to generate the folding potential. In this way, we hope to discriminate between breakup effects coming from the extended density and those resulting from the couplings to the continuum. The ^{6}He matter density is then given as a gaussian shape :

$$\rho(r) = C \exp(-br^2) \quad \text{fm}^{-3}. \tag{8}$$

Parameters in Eq. (8) were fixed to reproduce two versions of Gaussian density for ^{6}He which have rms radii of 2.54 fm (referred as the *ga* density) and 2.2 fm (*ro* density).

From a 'global' systematics for the WS imaginary potentials by Broglia and Winther [44], the values for the imaginary parameters can be calculated for the (A=6)+(A=12) system :

W_v=33.6 MeV, R_w = 4.394 fm (r_w=1.07 fm) and a_w= 0.63 fm. These values were used further as starting values to find the realistic absorption strength in ^{6}He+^{12}C system.

Results given by the real folded potential (calculated with the CDM3Y6 interaction and the *fc6* density) and the global parameters for the imaginary potential are plotted in Fig. 3. One can see that it is not possible to reproduce simultaneously the first deep minimum and the third maximum, even by varying the WS depth (see results obtained with $W = 20$ and 30 MeV). The systematics from Ref. [44] for the WS imaginary potentials is, therefore, only a rough approximation for the absorption in the ^{6}He+^{12}C case.

Concerning the strength of the real folded potential, the normalization factor N_r was found to be around 1.1-1.2 for elastic α-nucleus scattering, depending on the NN interaction used in the folding model [21, 27, 32]. The enhancement of the attractive real potential is, in fact, needed to reproduce the increase of cross sections at the larger angles (which represent the refractive part of the cross sections). On the other hand, it has been found by numerous folding analyses that $N_r < 1$ for light weakly-bound projectiles [45, 46]. For instance, in the case of ^{6}Li having the same number of nucleons as ^{6}He, the potential is reduced and the normalization factor was found to be around 0.5-0.6 [21]. It was shown by a Coupled -Channel method with Discretized Continuum [20] that the reduction of the interaction potential between ^{6}Li and various targets is mainly due to the break-up of the loosely bound ^{6}Li projectile. Such a reduction might be expected also in the case of the ^{6}He +^{12}C system. The folding analysis shows, however, that such a strong reduction is not observed in the ^{6}He+^{12}C case.

When the imaginary part is fixed to be W_v= 30.0 MeV, r_w= 1.07 fm (R_w= 4.39 fm) and a_w = 0.63 fm, the optimal N_r factor is about 1.18. For comparison, with a smaller depth, W_v= 20 MeV, the OM fit yields N_r = 1.1. It is clear that we have here a complex system in which the projectile combines two patterns : a tighly bound α-core and a low density part at large radii due to the halo. And the obtained normalization factor of the folded potential seems to reflect the competition between the break-up effects due to the weak binding of the ^{6}He nucleus and the refractive effects due to the α-core. When the parameters N_r, W_v, R_w, and a_w are optimized by the OM fit, we obtain smaller depths of the imaginary potential and N_r values close to 0.9, significantly larger than those found earlier for the ^{6}Li+^{12}C system. The results of the search for CDM3Y6, with gauss *ga* or *fc6* densities, and BDM3Y1 (*fc6*) are given in the table I. The corresponding cross sections are shown in Fig. 4. The first

minimum is well reproduced in all cases, and is very deep, but the data at larger angles are not correctly described. So the simple renormalization procedure is *not* appropriate in the ^{6}He+^{12}C case. The normalization globally affects the potential in the whole radial region while the measured elastic cross sections reveal two different patterns : the break-up which leads to the reduction of the cross sections and the enhanced cross sections at angles around 20° c.m due to the refractive α-core.

We compare, in Figs. 5 and 6, the real part of the potential calculated with BDM3Y1 or CDM3Y6, and with the different densities for ^{6}He. Both BDM3Y1 and CDM3Y6 interactions calculated with the same density for the ^{6}He nucleus (either the gaussian one, or the *fc6* one) lead to nearly the same potential (differences between the two are less than 1%). Therefore, all further discussions are based on results obtained with the CDM3Y6 density dependent interaction only. We show in Fig. 6 the folded CDM3Y6 potentials including either the *fc6* density, or the compact density *ga* (they have the same rms radius). The main differences between the two potentials are noticeable for radii greater than 4 fm, and are of the order of 10 % in this region. To understand these features, and to obtain meaningful values of the imaginary parameters, we need to compare the potential of the ^{6}He+^{12}C system to the α+^{12}C and ^{6}Li+^{12}C ones. Before studying the ^{6}Li+^{12}C potential which presents break-up effects, and to possibly better deduce the parameters of the total ^{6}He +^{12}C potential, we will consider the α+^{12}C potential to characterize the effect of the two neutron halo. Since we have a strong refractive pattern for α+^{12}C at larger angles, similar to the one observed for the ^{6}He+ ^{12}C, it is useful to compare the real and imaginary potentials obtained for ^{6}He on ^{12}C with those of α+^{12}C. We now examine a set of α+^{12}C data at different energies, in order to extract the potential at the energy of the ^{6}He + ^{12}C system, 38.3 MeV/nucleon.

B. ^{4}He + ^{12}C elastic scattering

The description of the elastic scattering by an interaction potential is ambiguous, due to the imaginary part and to the renormalization factor. The parameters of the volume imaginary part of the nucleus-nucleus potential must be determined phenomenologically. So the parameters deduced by the analysis are strongly dependent on the uncertainties in the normalization. A large data set, in terms of incident energy, is needed in order to reduce the uncertainties of the adjustment of N_r and of the imaginary part of the potential.

The aim is to have a consistent description of the normalization factor N_r of the real part and of the parameters (W_v, a_w, R_w) of the imaginary part, with respect to the energy. It will then be possible to predict the values at the energy of interest, for instance at 38.3 MeV/nucleon, and to calculate the elastic scattering at that energy with the folding model.

We examine the α + ^{12}C data measured at an energy of (in the laboratory frame) E_α = 104 MeV at the Karlsruhe Institute [47], at 139 MeV (34.75 MeV/nucleon) at the University of Maryland [48] and at 172.5 MeV (43.12 MeV/nucleon) at Julich [49].

The optical potential for the α + ^{12}C system is calculated by folding the effective interaction CDM3Y6 [27], with the matter density of the α particle and the two-parameter Fermi carbon density. The α density is given in Ref. [24] as a gaussian shape $\rho(r) = 0.4229 * exp(-0.7024r^2)$ fm^{-3}, whose rms radius is 1.46 fm. This radius is deduced from the charge density obtained by (e,e) scattering. The calculation is performed according to the prescriptions given in Ref.[32], with a realistic density dependence of the effective NN interaction together with the inclusion of the explicit treatment of the exchange potential, using a realistic local approximation.

We adjust the depth W_v, the radius R_w and the diffuseness a_w and the normalization N_r on the data. The values of N_r, W_v, R_w obtained for the sets of data, with the CDM3Y6 interaction, are given in Table II. The angular distributions obtained with these parameters are given in Fig. 7. The data are well reproduced. This analysis shows that for all the data N_r is of the order of 1.1 to 1.2. These variations may reflect the uncertainties on the normalization of the data. In fact this normalization factor should be constant at the different energies since the CDM3Y6 already contains an energy-dependent term.

A way to fix the normalization parameter is to use the volume integral of the potential, which has been shown to be a well-determined quantity of the elastic scattering data [35, 50]. The volume integral of the real potential per pair of interacting nucleons is given by the expression :

$$J_R = -\frac{4\pi N_r}{A_p A_t} \int U_F(u) u^2 du \tag{9}$$

where the normalization factor N_r of the data is taken into account. The value extracted at 104 MeV by model-independent calculations [51] is : $J_R/(4A) = -331 \pm 2$ MeV. fm^3. Therefore our description by the folding potential should give the same value. The volume

integral of the unrenormalized potential for CDM3Y6, is -284.3 MeV. fm^3 at 104 MeV, so we need $N_r = 1.165$. We keep this value for the various energies. The diffuseness a_w and the R_w are not expected to vary so much from one energy to another, so we fix them for all energies, in order to reach a global understanding of the α + ^{12}C potential. Of course, the best fit agreement is obtained by varying also R_w and a_w for each energy, but then we lose the global features that exist for these data from 104 MeV to 172.5 MeV. Here, by fixing the geometrical parameters, and letting only the depth W_v vary freely in the search, the variation of W_v with the energy can be clearly determined, as shown by the table III. Data at the three energies are well reproduced in the Fig. 8 with the same values for the radius ($R_w = 3.76$ fm, the reduced radius is : 0.97 fm) and the diffuseness ($a_w = 0.6$ fm). Then the depth has a range of 19 to 22.5 MeV (table III).

At the energy of the ^{6}He+^{12}C system, which is 38.3 MeV/nucleon (153.2 MeV for the ^{4}He+^{12}C system), the values expected for the potential are : $N_r = 1.165$, $R_w = 3.76$ fm, $a_w = 0.6$ fm and, by interpolating the imaginary depth between the values obtained at 139 MeV and at 172.5 MeV, W is equal to 21.8 MeV.

In Fig. 9, the folded potential for ^{4}He +^{12}C with the CDM3Y6 interaction (normalized with 1.165) is compared to the one calculated with CDM3Y6 and the gaussian *ro* density for the ^{6}He +^{12}C system.

The imaginary part of the potential obtained for ^{4}He +^{12}C will be tested for ^{6}He +^{12}C, taking the appropriate geometry (same reduced r_w radius, but now multiplied by $6^{1/3}$+$12^{1/3}$). The break-up effects will not be taken into account by means of the normalization factor, but rather by simulating the polarization potential considered in Sec. I.

IV. SIMPLE ESTIMATE OF THE POLARIZATION POTENTIAL

We have seen in the previous Section that a simple renormalization procedure for the real folded potential has failed to reproduce the new elastic ^{6}He+^{12}C data over the whole angular range. It is clear that a more accurate fine-tuning of the strength of the real folded potential is needed. For this purpose we recall that, according to the Feshbach theory of microscopic optical potential [19], the nucleus-nucleus optical potential is expressed in general as

$$U = U_{00} + \Delta U_{pol}, \tag{10}$$

where ΔU_{pol} is the so-called dynamical polarization potential which is complex, non-local and energy dependent :

$$\Delta U_{pol} = \lim_{\varepsilon \to 0} \sum_{\alpha,\alpha' \neq 0,0} V_{0\alpha} \left(\frac{1}{E - H + i\varepsilon} \right)_{\alpha\alpha'} V_{\alpha' 0}. \tag{11}$$

The first term in (10) describes the projectile-target interaction with the two nuclei remaining in their ground states ϕ_{p0} and ϕ_{t0} :

$$U_{00} = (\phi_{p0}\phi_{t0} \mid v_{\rm NN} \mid \phi_{p0}\phi_{t0}), \tag{12}$$

where $v_{\rm NN}$ is the effective in-medium NN interaction.

U_{00} can be represented by the folding potential U_F given by Eq. 1, i.e., $U_{00} \equiv U_F$.
The polarization potential ΔU_{pol} represents higher-order contributions to the optical potential from all inelastic channels that are allowed energetically. It affects the potential U_{00}, describing the elastic scattering, through virtual processes : the interacting system may be excited from the ground state to the α state, and then makes a transition to the α' state, finally decaying from α' to ground state. The complex ΔU_{pol} is the main source of the imaginary part W of the optical potential. With $\Delta U_{pol} = V_{pol} + iW_{pol}$ as the polarization potential (V_{pol} and W_{pol} real), the total optical potential can be written as :

$$U = U_{00} + \Delta U_{pol} = U_F(CDM3Y6) + V_{pol} + iW$$

with W including W_{pol}.
For well-bound nuclei, the probability of excitation during the elastic scattering is weak, and the contribution of the ΔU_{pol} to the real optical potential is about an order of magnitude smaller than the real folded potential U_F [21]. A slight renormalization of the real folded potential by the factor N_r is a convenient way to take into account effectively the DPP contributions.

The weaker the binding energy of the nucleus, along with a high probability of a transition to the excited or clustering states, the greater the influence of ΔU_{pol}. In the cases of loosely bound projectiles, such as ^{6,11}Li, the simple renormalization procedure was shown to be less accurate and one needs to explicitly add the DPP to the real folded potential [23, 46].

It is well established now that for the loosely bound projectiles, the breakup effects contribute to the DPP strongest at the surface region [20, 23, 52]. Based on the results

of microscopic studies within various coupled reaction channel models, a complex surface potential $\Delta U_{pol} = V_{pol} + iW_{pol}$, with a repulsive real part, can be used to simulate the surface effects caused by the polarization potential [9, 23, 53]. In this work, we assume that both the real (repulsive) and imaginary parts of ΔU_{pol} have the same radial shape, i.e., $V_{pol}(R) = -V_{pol} f(R)$ and $W_{pol}(R) = -W_{pol} f(R)$, where

$$f(R) = \exp\Big(\frac{R - R_{pol}}{a_{pol}}\Big)/[1 + \exp\Big(\frac{R - R_{pol}}{a_{pol}}\Big)]^2. \tag{13}$$

Here $V_{pol} \leq 0$. Such a parametric form of the complex DPP has been used recently [9] in the OM analysis of the elastic ^{6}He scattering data on proton target. Note that the repulsive surface term leads to the reduction of the real optical potential, which explains the best fit normalization $Nr < 1$ found for the loosely bound projectiles [20, 23, 46, 52]. This is one of the most important coupling effect found in the elastic channel due the breakup.

The parameters of the phenomenological polarization potential can be related to the microscopic approach by considering the value of the potential at the surface, as has been done by Khoa *et al.* in Ref. [23] for the ^{11}Li+^{12}C system. The DPP parameters (V_{pol}, W_{pol} and a_{pol}) were fixed to give values of $V_{pol}(R)$ and $W_{pol}(R)$, at R = 6.5 fm, close to those obtained in the microscopic coupled discretized channel calculations performed in Ref [52]. Here, we have obtained elastic data without any inelastic contribution, therefore we can consider the DPP parameters for ^{6}He+^{12}C system as free parameters which will be adjusted to the best OM fit to the data. In our study, we provide the phenomenological form for the ^{6}He+^{12}C DPP.

Both interactions, BDM3Y1 and CDM3Y6 give similar potentials ^{6}He+^{12}C whether the folding is done with the compact density ("gauss") or with the halo (fc6) one, as was seen in Sec. III A. CDM3Y6 has given good results for α+^{12}C. So, we turn now to the analysis of the elastic scattering for ^{6}He retaining only the CDM3Y6 interaction.

At the first step, U_{pol} can be taken without a radius ($R_{pol} = 0$) as attempted earlier by Hussein and Satchler [53]. To further explore the sensitivity of the data to the real optical potential, we have put $W_{pol} = 0$ and tried to adjust the depth V_{pol} and diffuseness a_{pol} of the real part of the DPP and parameters of the WS imaginary potential to the best OM fit. A very satisfactory agreement with the data (see Fig. 10) was reached with unrenormalized real folded potential added to a real DPP with $V_{pol} = -64$ MeV, $a_{pol} = 1.33$ fm, and a WS imaginary potential given by $W_v = 19$ MeV, $r_w = 1.13$ fm, and $a_w = 0.63$ fm. Thus, we

have assumed in this case that effects coming from the imaginary DPP are implicitly taken into account by the best-fit WS imaginary potential.

Figure 10 compares the data with the two calculated cross sections obtained with and without the DPP (the dashed and the solid curves, respectively). Without renormalizing the real part, and with no DPP, the best fit was obtained with an imaginary part corresponding to W_v=20 MeV, r_w = 1.13 fm and a_w =0.63 fm, very close to the one obtained in the description of α + ^{12}C elastic scattering at 38.3 MeV/nucleon. The same is taken for the calculation with the gaussian *ro* density. One can see that the (real) DPP added to the original ^{6}He+^{12}C folded potential leads to a good description of both the first minimum and the third maximum in the measured data, which has not been achieved by a simple renormalization procedure for the folded potential.

The total (real) potential including the DPP is plotted in Fig. 11 and compared to both the unrenormalized and normalized folded potentials obtained with the Gaussian density *ga*. At the surface ($R \simeq 4-5$ fm) the total potential with the DPP is very close to the normalized folded potential, while it is shallower than the folded potential at smaller distances. To show the effects of the two-neutron halo in ^{6}He+^{12}C system, we have also plotted the real folded potential for α+^{12}C system at the same energy (normalized by a factor N_r = 1.165 as given by the systematics from Sec. III B). One can see that the total α+^{12}C and ^{6}He+^{12}C potentials have about the same depths but differ strongly at the surface region, where the contribution given by the two halo neutrons is significant. Results of the same OM calculations using the *fc6* density instead of the Gaussian density are presented in Fig. 12, and one has about the same effect of the polarization potential.

Nevertheless, the adopted shape for the DPP is very simple. In order to have a more physical description of the DPP, it is necessary to explore other possible choices for the DPP with nonzero value of the radius R_{pol}, in order to better determine the effect of the couplings on the interaction potential. To get a precise idea of the value of the radius R_{pol}, it is helpful to study a system which exhibits similarities with the ^{6}He +^{12}C case and the same mass numbers, like the ^{6}Li +^{12}C system. ^{6}Li is more tighly bound than ^{6}He but it also presents interesting cluster features : it is known to be easily broken up to the α and deuteron clusters. All its excited states are above the $S_{\alpha+d}$ separation energy of 1.475 MeV, they are unbound and can decay into clusters. So their excitation by the nuclear and Coulomb field of a target leads to the break-up of the ^{6}Li nucleus. The Coupled Discretized Continuum

Channels (CDCC) methods have been successful in showing how the breakup of the ^{6}Li projectile into α and d clusters affects the elastic scattering on different targets [20].

Data for the elastic scattering of ^{6}Li on a carbon target exist at different energies, giving the opportunity to consistently fix the parameters of the imaginary part and of the polarization potential for the whole data set, as explained in the next Section. The features of the DPP for ^{6}He+^{12}C will then be deduced from those of ^{6}Li+^{12}C.

V. CONSISTENT POLARIZATION POTENTIAL FOR ^{6}LI, ^{6}HE +^{12}C SYSTEMS

A. Analysis of the ^{6}Li +^{12}C elastic scattering data and extraction of the DPP at 38.3 MeV/nucleon

Previous folding analysis [46] performed for the ^{6}Li+^{12}C system has clearly indicated the need for an appropriate DPP to be added to the folded potential. In Ref. [46], the folded potential was calculated with the BDM3Y1 NN interaction. The present analysis is made with the folding model incorporating the CDM3Y6 interaction and we consider again the elastic ^{6}Li+^{12}C data measured at 16.5 MeV/nucleon [54], 26 MeV/nucleon [55], 35 MeV/nucleon [56], and 53 MeV/nucleon [57]. The proton density of ^{6}Li used in the folding calculation is constructed as described in [24] : the charge density of ^{6}Li is extracted from (e,e) scattering [58], unfolded from the finite size of the proton, and the neutron density is assumed to be the same as the proton one. The rms radius of the matter density obtained in this way is 2.43 fm.

Without any polarization potential, these data require a strong renormalization of the real folded potential to be correctly described, as shown in Fig. 13. The normalization factor and the parameters of the imaginary potential can be found in Table IV. At the lower energy of 99 MeV, the best-fit normalization factor $N_r \approx 0.56$ is quite different from those obtained at higher energies. The data set at 99 MeV is, therefore, treated separately from the energy range of 156–318 MeV for which some kind of systematic behavior can be found, with the same N_r factor of about 0.85 and a diffuseness a_w around 0.6 fm.

As was the case for α+^{12}C, the normalization factor should not change with the energy, at least for the higher energies. This corresponds to the fact that for energies E $\geq$ 26 MeV, break-up effects depend weakly on the energy but increase strongly at lower energies (E

$\leq$ 20 MeV).

By fixing $N_r = 0.85$ and $a_w = 0.6$ at 156–318 MeV (see Table V) in the OM search, the reduced radius r_w of the WS imaginary potential seems to move around 0.90–0.97. At 99 MeV, the first search had given a small value for the radius of the imaginary part. In a second step, a more realistic R_w value was searched. It gives a higher χ_2 value but the agreement with the data was still satisfactory. The table V summarizes the result of the search for the parameters of the imaginary part W_v and R_w that give the best fit, together with the fixed N_r and a_w values. These parameters give a reasonable description of the data, as shown in Fig. 14.

It can be seen that the renormalization procedure for the real folded potential is not sufficient to describe the cross sections at large angles (above 30° c.m.) which correspond to the refractive region. Even if all the parameters (N_r, W_v, a_w, and R_w) are freely released in the search, the large-angle data are not well reproduced at 99 and 156 MeV, as shown in Fig. 13. So the renormalization procedure does not give the right refractive scattering pattern, which is very sensitive to the real optical potential at small radii, as was shown in Ref. [59]. This means that the renormalization procedure, which reduces the potential on the whole radial range, does not give a correct potential at small internuclear distances. Therefore it is here better to use the polarization potential, which reduces the folding potential mostly at radii around 4-5 fm, as shown in the earlier folding analysis by Khoa *et al.* [46] of the same ^{6}Li+^{12}C data. In Ref. [46], a spline shape has been used to estimate the strength and shape of the DPP. In our analysis, we adopt for the DPP the surface term defined in section IV and add it to the folded potential calculated with CDM3Y6. We choose to fix the value of the radius R_{pol}, by taking $R_{pol} \simeq R_{1/2}$ with $R_{1/2}$ corresponding approximately to the radius at which the strength of the folded potential at small radii is divided by a factor two. Hence, $R_{1/2}$ is obtained from the $U_F(R_{1/2}) = U_F(0)/2$ relation. So R_{pol} is taken equal to 2.85 fm, and this value is then fixed in the calculations including the DPP for the four sets of data. The reduced radius of the imaginary part r_w is also fixed at its value obtained for 318 MeV in the previous adjustment (see table V). The value of the diffuseness a_{pol} of the DPP turned out to be weakly dependent on the energy and can be fixed at a value of 0.95. The same was done with the depth of the WS imaginary potential for the energies of 156, 210 and 318 MeV. We adjust the depths of V_{pol} and W_{pol} in order to get a good agreement with the data in Fig. 15. All the obtained OM parameters and those of the DPP

are given in Tab. VI.

It is interesting to compare the real potentials used to reproduce the data : the renormalized ^{6}Li+^{12}C folded potential, the total potential including the DPP (solid curve), with the unrenormalized one and the normalized α +^{12}C potential, at the same energy per nucleon. Figs. 16 and 17 present this comparison for 99 MeV (16.5 MeV/nucleon) and 210 MeV (35 MeV/nucleon), respectively. With our choice for R_{pol}, the DPP for ^{6}Li+^{12}C reduces mostly the potential at radii around 4-5 fm, and slightly modifies the potential for radii lower than than 2 fm. The contribution of the (real) DPP to the total real optical potential is of the order of 15% at 26, 35 and 53 MeV/nucleon (see Fig. 17) and reaches 40% at the smaller energy of 16.5 MeV/nucleon (Fig. 16). The total potential ($U_F + \mathrm{Re}\Delta U_{pol}$) and the normalized folded potential ($N_r U_F$) have nearly the same values at the surface, i.e., for R $\simeq$ 4-5 fm. These features of the DPP are in agreement with Sakuragi's theoretical conclusions [20], concerning the analysis of the elastic scattering of ^{6}Li on different targets, within the framework of the microscopic CDCC calculations. We thus have obtained an imaginary potential for the ^{6}Li+^{12}C system, which is consistent with the data at 26, 35 and 53 MeV/nucleon. It is reasonable to use it as an imaginary volume part for the ^{6}He+^{12}C system.

B. Discussions of the DPP in the ^{6}He+^{12}C system

We have made further OM analysis of the elastic ^{6}He+^{12}C data based on the WS imaginary potential that has the same depth and radius as found in ^{6}Li+^{12}C case. All other parameters were searched for the best fit to the data. OM results obtained with the real optical potentials folded with the Gaussian density *ga* and the density from the 3-body model *fc6* (which have the same rms radii of 2.54 fm) are compared with the data in Figs. 18 and 19, respectively. Values of the DPP U_{pol} and of the imaginary part W are given in the table VII.

The agreement with the data is reasonable in both cases, with a slightly better fit to the data points around the first minimum given by the folded potential based on Gaussian density. If we look at the shape of the real optical potentials plotted in Figs. 20 and 21 for these two cases, we find that the total potentials ($U_F + \mathrm{Re}\Delta U_{pol}$) have about the same strength at the surface, around 5 fm. From a comparison with the total ^{6}Li+^{12}C and

^{4}He+^{12}C potential (see the thick-dash, dotted and solid lines in Figs. 20 and 21) one can see that the ^{6}He+^{12}C potential is more attractive at the surface (4 to 6 fm) which is clearly due to the extended tail of the ^{6}He density. For radii larger than 3 fm, the DPP U_{pol} reduces the folding U_F potential by nearly 40 %, as can be seen in Fig. 20. The comparison between the results obtained with the gaussian and the *fc6* density underscores the role played by the halo on the scattering. It mainly induces break-up effects incorporated in the DPP, and the tightly bound Alpha core leads to refractive effects at larger angles. A better treatment could be reached by working with a more sophisticated function to simulate the DPP, than the simple surface shape used here. For instance, a transition potential could be generated to take into account the soft dipole and quadrupole modes of the ^{6}He as described in Ref. [60] and incorporated in our coupled-channel calculations. However, the simple shape of the complex DPP found for the ^{6}He+^{12}C system provides a realistic estimate for the contribution from the DPP to the 'bare' ^{6}He+^{12}C optical potential. It is a practical tool to describe and understand the elastic scattering of a halo nucleus.

VI. CONCLUSIONS

In the present article, we have presented the new extended data for elastic scattering of ^{6}He on ^{12}C target, without any contamination from target excitations. These data were analyzed in the OM to find information about the optical potential between a halo nucleus and a target.

The real part of the ^{6}He+^{12}C interaction potential was calculated in the framework of the folding model, including new density-dependent NN interactions, BDM3Y1 and CDM3Y6, whose density-dependence accounts for the saturation properties of the nuclear matter. Both shapes for the NN interaction give similar folded potentials for ^{6}He on ^{12}C. In Ref. [27], these interactions were demonstrated to be well-adapted for the study of refractive elastic scattering of light nuclei such as α, ^{12}C and ^{16}O. With the analysis of the ^{6}He data we show that they are also well-suited to the study of the elastic scattering of a light exotic nucleus, provided " some account is taken of the very important dynamic polarization potential (DPP) due to break-up ", as pointed out by Satchler and Brandan [21]. In our analysis, a complex surface potential, with a repulsive real part, was indeed added to the 'bare' optical potential generated by the folding model in order to simulate the surface effects induced by

the polarization potential.

Our data and the ^{6}Li+^{12}C data demonstrate that the break-up effects on elastic scattering do not simply correspond to a global renormalization of the potential ; the DPP is needed to correctly describe the whole angular range of the cross sections. With a consistent absorption potential found for both ^{6}Li+^{12}C and ^{6}He+^{12}C systems at the same energy, the DPP was shown to affect the total optical potential strongly at the surface, at radii around 4-5 fm. This trend agrees with the theoretical results given by various Coupled Reaction Channel models. In this way, our study also provides a handy shape of the DPP, which might be useful in other investigations of breakup effects in elastic scattering of loosely-bound projectiles.

Predicted cross sections for angles larger than 23° c.m. (see Fig. 18 and 19) are different if one uses different types of the ^{6}He density. New measurements are needed to improve the statistical precision in the region between 15 and 22° c.m. and to measure cross sections at larger angles, to provide more precise data for the future test of different nuclear structure models. In this kind of analysis, it is crucial to have data at different energies ranging from 25 to 100 MeV/nucleon, and on different targets, in order to systematically study the optical potential and find the general trends of the DPP, as was done for ^{6}Li.

Theoretical calculations of the DPP by Coupled Reaction Channel models, with a microscopic description of the ^{6}He excitations to the cluster states and to the continuum, are strongly encouraged. The weak binding of the exotic nuclei involves an increase of the break-up probabilities, and this effect must be taken into account to deduce information on the structure of halo nuclei through the study of reaction mechanisms at low energy. Moreover, the comparison between data and the theories proposed to estimate the effects of the continuum will enhance our knowledge on the channels coupled to the continuum.

Acknowledgments

We thank Dr I. J. Thompson for providing us with his ^{6}He density distributions and Dr A. Lumbroso for helpful comment. The assistance of the SPEG crew in the preparation of the experiment is gratefully acknowledged. One of the authors (D.T.K.) was supported by

[1] I. Tanihata, *Proceedings of the 7th International Conference on Nucleus-Nucleus collisions, Strasbourg, France July 3-7th 2000*, published in Nucl. Phys. **A685**, 80c (2001) ; B. M. Sherrill, *ibid.*, **A685**, 134c (2001).

[2] I. Tanihata, Phys. Lett. B **160**, 380 (1985) ; *ibid.*, B **206**, 592 (1988).

[3] P. G. Hansen and B. Jonson, Europhys. Lett. **4**, 409 (1987).

[4] Y. Ogawa, K. Yabana and Y. Suzuki, Nucl. Phys. **A543**, 722 (1992).

[5] M. V. Zhukov, B. V. Danilin, D. V. Fedorov, J. M. Bang, J. Thompson and J. S. Vaagen, Phys. Rep. **151**, 299 (1993).

[6] I. Tanihata, D. Hirata, T. Kobayashi, S. Shimoura, K. Sugimoto, and H. Toki, Phys. Lett. B **289**, 261 (1992).

[7] G. D. Alkhazov *et al.*, Phys. Rev. Lett **78**, 2313 (1997).

[8] A. A. Korsheninnikov *et al.*, Nucl. Phys. **A617**, 45 (1997)

[9] V. Lapoux *et al.*, Phys. Lett. B **517**, 18 (2001).

[10] R. Wolski *et al.*, Phys. Lett. B **467**, 8 (1999).

[11] T. Aumann *et al.*, Phys. Rev. C **59**, 1252 (1999).

[12] A. Lagoyannis *et al.*, Phys. Lett. B **518**, 27 (2001).

[13] L. V. Chulkov, B. V. Danilin, V. D. Efros, A. A. Korshenninikov and M. V. Zhukov, Europhys. Lett **8**, 245 (1989).

[14] B. V. Danilin, I. J. Thompson, M. V. Zhukov, J. S. Vaagen and J. M. Bang, Phys. Lett. B **333**, 299 (1994) ; S. N. Ershov, T. Rogde, B. V. Danilin, J. S. Vaagen, I. J. Thompson and F. A. Gareev, Phys. Rev. C **56**, 1483, (1997).

[15] E. Nielsen, D. V. Fedorov, A. S. Jensen, and E. Garrido, Phys. Rep. **347**, 373 (2001).

[16] B. S. Pudliner, V. R. Pandharipande, J. Carlson, S. C. Piper and R. B. Wiringa, Phys. Rev. C **56**, 1720 (1997) ; S. C. Pieper, V. R. Pandharipande, R. B. Wiringa, and J. Carlson, *ibid.*, C **64**, 014001 (2001).

[17] J. S. Al-Khalili, J. A. Tostevin, Phys. Rev. C **57**, 1846 (1998).

[18] J. A. Tostevin and J. S. Al-Khalili, Nucl. Phys **A616**, 418c (1997).

[19] H. Feshbach, Ann. Phys. **5**, 357 (1958), *Theoretical Nuclear Physics (Wiley, New York 1992).*

[20] Y. Sakuragi, Phys. Rev C **35**, 2161 (1987).

[21] M. E. Brandan and G. R. Satchler, Phys. Rep. **285**, 143 (1997).

[22] K. Arai, Y. Suzuki and R. G. Lovas, Phys. Rev. C **59**, 1432 (1999).

[23] D. T. Khoa, G. R. Satchler, and W. von Oertzen, Phys. Lett. B **358**, 14 (1995).

[24] G. R. Satchler and W. G. Love, Phys. Rep. **55**, 183 (1979).

[25] J. S. Al-Khalili *et al.*, Phys. Lett. B **378**, 45 (1996).

[26] J. J. Kolata *et al.*, Phys. Rev. Lett. **69**, 2631 (1992).

[27] D. T. Khoa, G. R. Satchler, and W. von Oertzen, Phys. Rev. C **56**, 954 (1997).

[28] L. Bianchi *et al.*, NIM **A 276** (1989) 509-520.

[29] A. Joubert *et al.*, Particle Accelerator Conference IEEE Vol 1 (1991) 594.

[30] J. L. Baelde *et al.*, Nouvelles du GANIL, n^0 44, fév. 1993.

[31] M. Mac Cormick *et al.*, rapport GANIL **R98-02** 1998.

[32] D. T. Khoa, Phys. Rev. C **63**, 034007 (2001).

[33] B. Sinha, Phys. Rep. **20**, 1 (1975); B. Sinha and S. A. Moszkowski, Phys. Lett. **81B**, 289 (1979).

[34] N. Anantaraman, H. Toki, and G. F. Bertsch, Nucl. Phys. **A398**, 269 (1983).

[35] G. R. Satchler, Direct Nuclear Reactions, Oxford Univ. Press., Oxford, 1983.

[36] M. E. Brandan and K. W. Mc Voy, Phys. Rev. C **55**, 1362 (1997).

[37] G. R. Satchler and D. T. Khoa, Phys. Rev. C **55**, 285 (1997).

[38] M. E. Brandan and G. R. Satchler, Nucl. Phys **A487**, 477 (1988).

[39] J. Raynal, Phys. Rev. C **23**, 2571 (1981).

[40] D. T. Khoa, W. von Oertzen, Phys. Lett. B **342**, 6 (1995).

[41] D. T. Khoa, W. von Oertzen and H. G. Bohlen, Phys. Rev. **C 49**, 1652 (1994).

[42] M. El-Azab Farid and G. R. Satchler, Nucl. Phys. **A438**, 525 (1985).

[43] J. S. Al-Khalili, J. A. Tostevin and I. J. Thompson, Phys. Rev. C **54**, 1843 (1996).

[44] R. A. Broglia and A. Winther, *Heavy Ions Reactions, Lectures notes*, **vol I** : Elastic and Inelastic Reactions, the Benjamin/Cummings Publishing Company, Inc., 1981.

[45] N. Alamanos and P. Roussel-Chomaz, Ann. Phys. Fr. vol **21**, 601 (1996).

[46] D. T. Khoa, G. R. Satchler and W. von Oertzen, Phys. Rev. C **51**, 2069 (1995).

[47] G. Hauser, R. Löhken, H. Rebel, G. Schatz, G. W. Schweimer and J. Specht, Nucl. Phys. **A128**, 81 (1969).

[48] S.M. Smith et al., Nucl. Phys. **A207**, 273 (1973).

[49] A. Kiss, C. Mayer-Böricke, M. Rogge, P. Turek and S. Wiktor, J. Phys. G **13**, 1067 (1987).

[50] D. Jackson and R. C. Johnson, Phys. Lett. B **49**, 249 (1974).

[51] C. J. Batty et al., Adv. Nucl. Phys. 19/1 (1989).

[52] K. Yabana, Y. Ogawa and Y. Suzuki, Phys. Rev. C **45**, 2909 (1992).

[53] M. Hussein and G. R. Satchler, Nucl. Phys. **A567**, 165 (1994).

[54] P. Schwandt, W. W. Jakobs, M. D. Kaitchuck, P. P. Singh, W. D. Ploughe, F. D. Becchetti and J. W. Jänecke, Phys. Rev. C **24**, 1522 (1981).

[55] J. Cook, H. J. Gils, H. Rebel, Z. Majka, and H. Klewe-Nebenius, Nucl. Phys. **A388**, 173 (1982).

[56] A. Nadasen, M. Mc Master, G. Gunderson, A. Judd, S. Villanueva, P. Schwandt, J. S. Winfield, J. van der Plicht, R. E. Warner, F. D. Becchetti and J. W. Jänecke, Phys. Rev. C **37**, 132 (1988).

[57] A. Nadasen, T. Stevens, J. Farhat, J. Brusoe, P. Schwandt, J. S. Winfield, G. Yoo, N. Anantaraman, F. D. Becchetti, D. Brown, D. Hotz, J. W. Jänecke, D. Roberts, R. E. Warner, Phys. Rev. C **47**, 674 (1993).

[58] G. C. Li, I. Sick, R. R. Whitney and M. R. Yearian, Nucl. Phys. **A162**, 583 (1971).

[59] G. R. Satchler, Nucl. Phys. **A409**, 3c (1983).

[60] S. Funada, Prog. of Theo. Phys. **vol 93**, No. 2 (1995).

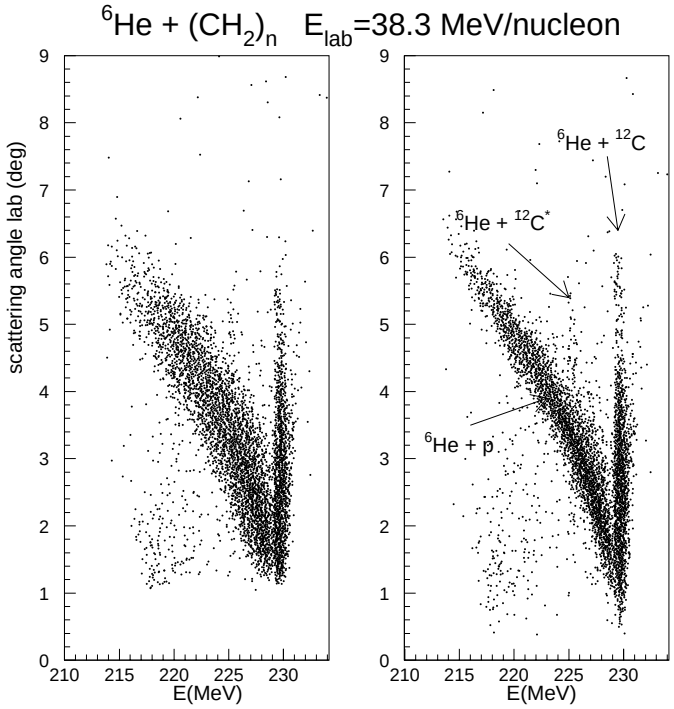

FIG. 1: Spectra of the scattering angle of the ^{6}He at 38.3 MeV/nucleon on a polypropylene target in the focal plane of the SPEG spectrometer (at 3.5°) as a function of the energy loss. In the spectrum on the left-hand side, the angle is calculated by assuming that the incident beam is perpendicular to the target. In the second one, on the right-hand side, the incident angle given by the beam detectors is taken into account.

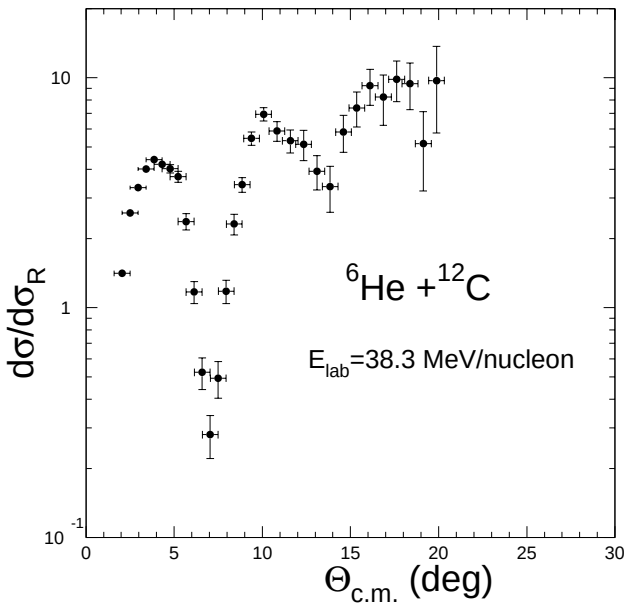

FIG. 2: Elastic scattering data for ^{6}He on ^{12}C at 38.3 MeV/nucleon. Experimental differential cross sections are divided by the Rutherford cross sections.

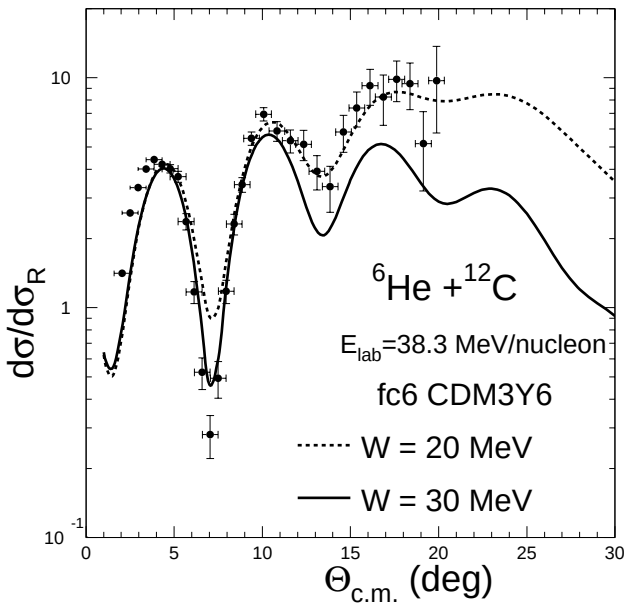

FIG. 3: Elastic scattering data for ^{6}He on ^{12}C at 38.3 MeV/nucleon in comparison with the results given by the real folded potential(obtained with the CDM3Y6 interaction and the *fc6* density). r_w and a_w values of the imaginary part are equal to 1.07 fm and 0.63 fm. The solid and dashed lines are obtained with an imaginary depth W_v equal to 30 MeV and W_v= 20 MeV, respectively.

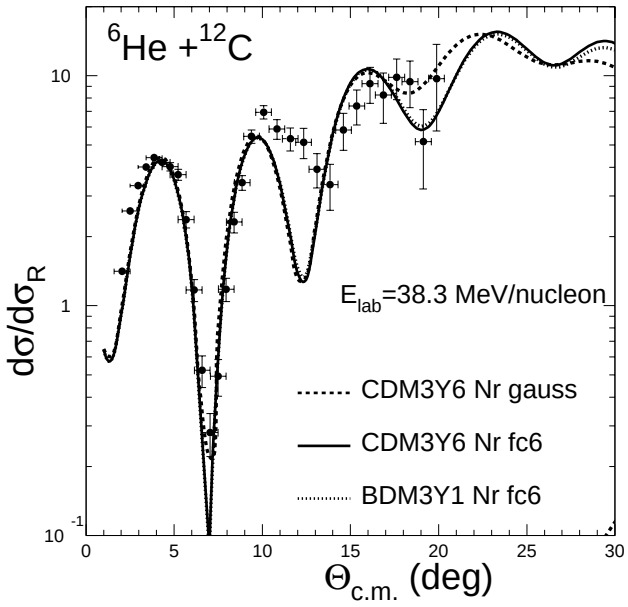

FIG. 4: Elastic scattering data for ^{6}He on ^{12}C at 38.3 MeV/nucleon in comparison with the OM results given by the real folded potential. The solid (dotted) curve is obtained with the CDM3Y6 (BDM3Y1) interaction and the *fc6* density. The dashed curve is obtained with the CDM3Y6 interaction and the gaussian-shape density (*ga*) for ^{6}He. The normalization factor and the parameters of the imaginary part are explained in the text and given in Tab. I.

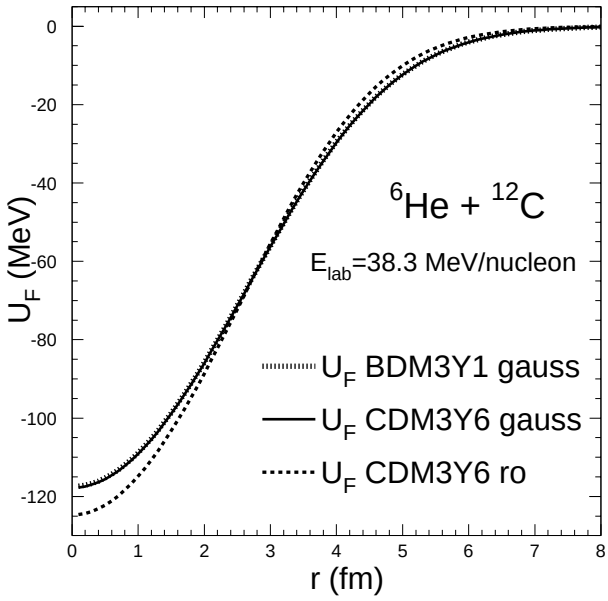

FIG. 5: Real folded potentials calculated with the CDM3Y6 (solid line) and BDM3Y1 (dotted curve) interactions, for the elastic scattering of ^{6}He+^{12}C at 38.3 MeV/nucleon. The gaussian density *ga* was used for ^{6}He. The dashed curve is the folded potential for ^{6}He +^{12}C calculated with CDM3Y6 and the gaussian *ro* density.

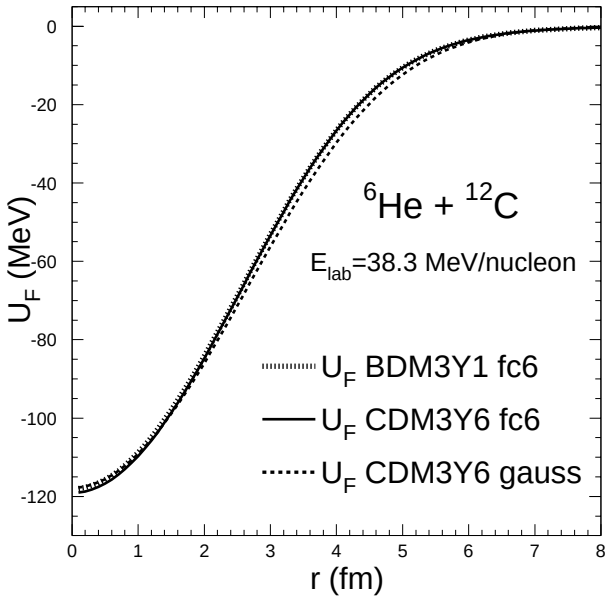

FIG. 6: Real folded potentials calculated with CDM3Y6 for the ^{6}He+^{12}C system at 38.3 MeV/nucleon. The solid line is for the interaction potential obtained with the *fc6* density and the dashed line is calculated with the gaussian density *ga*. The dotted curve is the folded potential calculated with BDM3Y1 and the *fc6* density.

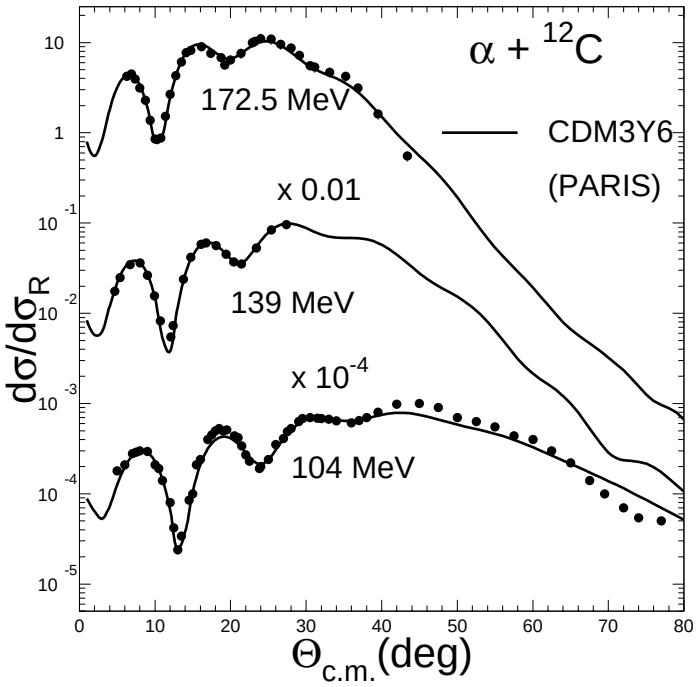

FIG. 7: Elastic scattering data for $\alpha + {}^{12}$C, at 104 MeV, 139 MeV and 172.5 MeV, are reproduced using the renormalized real folding potential calculated using the CDM3Y6 interaction and with the adjustment of the imaginary part as indicated in the text.

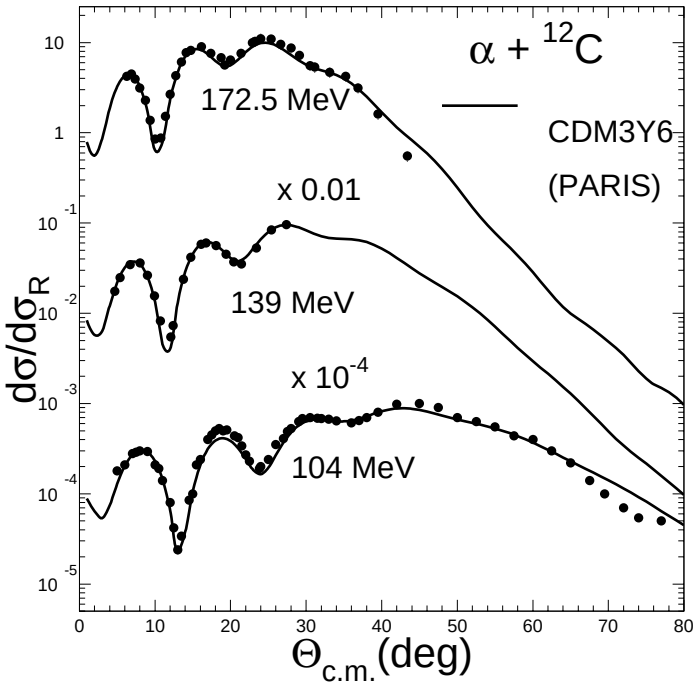

FIG. 8: Elastic scattering data for $\alpha + {}^{12}$C, at 104 MeV, 139 MeV and 172.5 MeV, are reproduced with the renormalization of the real folding potential calculated using the CDM3Y6 interaction and with the adjustment of the depth of the imaginary part as indicated in the text. For the three sets of data, the normalization factor of the real part is fixed at 1.165, and the values of the diffuseness and radius of the imaginary part are 3.76 fm and 0.6 fm, respectively.

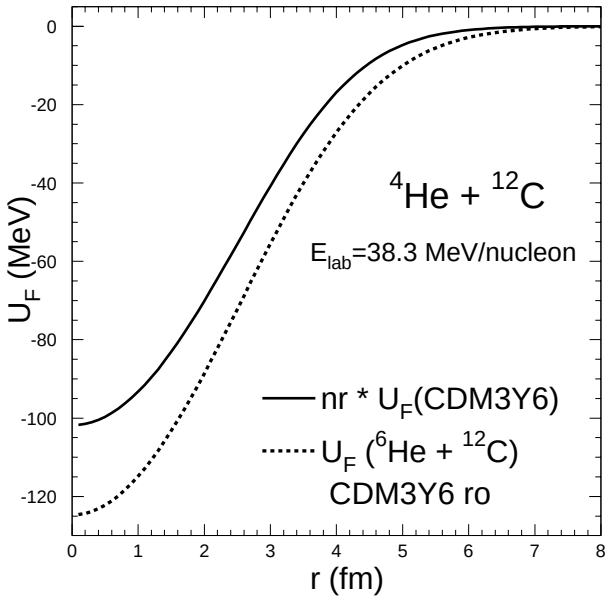

FIG. 9: Real folded potentials calculated with CDM3Y6 (solid line) for the system ^{4}He+^{12}C at 38.3 MeV/nucleon. The ^{4}He+^{12}C potential is normalized with the factor N_r (equal to 1.165) obtained in the analysis of the elastic scattering of α on ^{12}C. The density incorporated in the folded potential is indicated in the text. The dashed curve represents the folded potential for ^{6}He $+^{12}$C calculated with CDM3Y6 and the gaussian *ro* density at 38.3 MeV/nucleon.

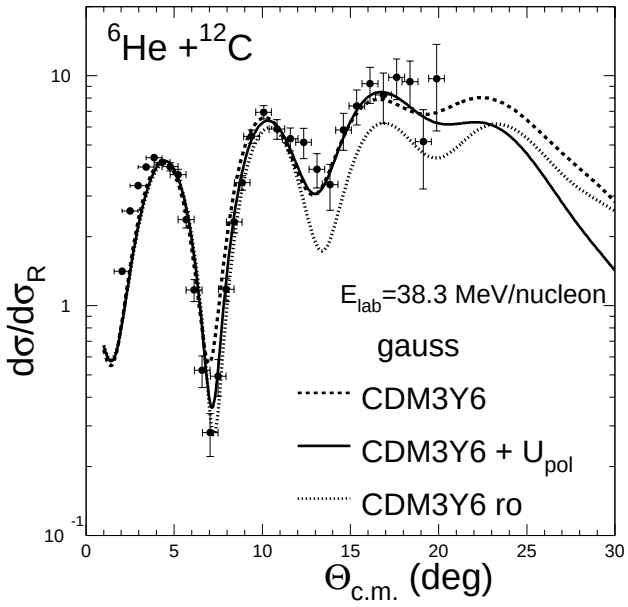

FIG. 10: Elastic scattering for ^{6}He + ^{12}C at 38.3 MeV/nucleon in comparison with the OM results given by the real folded potential (obtained with the CDM3Y6 interaction and the gaussian *ga* density for ^{6}He). The dashed curve is obtained with the unrenormalized folded potential only. The solid curve is obtained by adding a complex surface polarization potential to the real folded potential. Its parameters, and those of the imaginary part, are explained in the text. The dotted line is obtained by folding the CDM3Y6 interaction with the compact gaussian density *ro*.

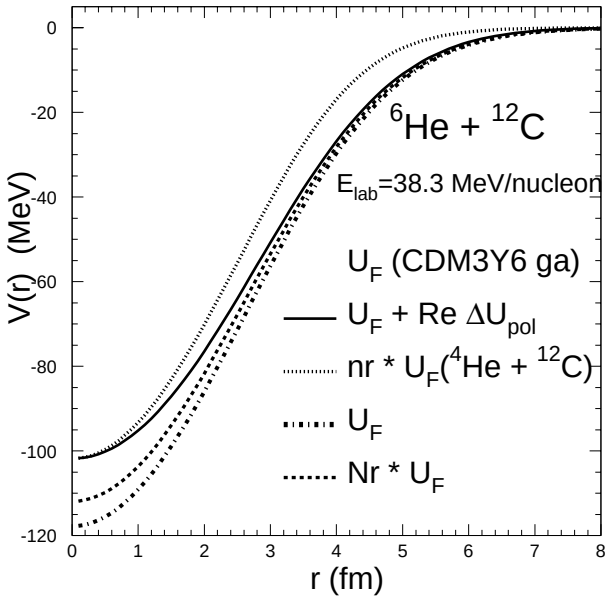

FIG. 11: Real folded potentials calculated with CDM3Y6 and the gaussian density *ga*, for the elastic scattering of ^{6}He+^{12}C at 38.3 MeV/nucleon. The folded potential U_F is represented with the dash-dotted line. The renormalized potential with the factor N_r given in Table I is represented with the long-dashed curve. The total potential obtained by adding the polarization potential to U_F is drawn with the solid curve. For comparison, the CDM3Y6 potential for the ^{4}He+^{12}C system at 38.3 MeV/nucleon (normalized with the factor $n_r = 1.165$ deduced in section III) is also presented, with the dotted line.

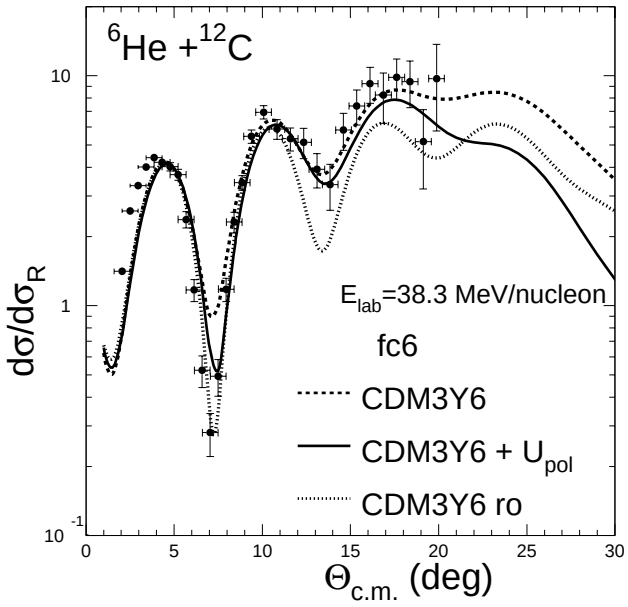

FIG. 12: The same as for Fig. 10 but using the *fc6* density for ^{6}He.

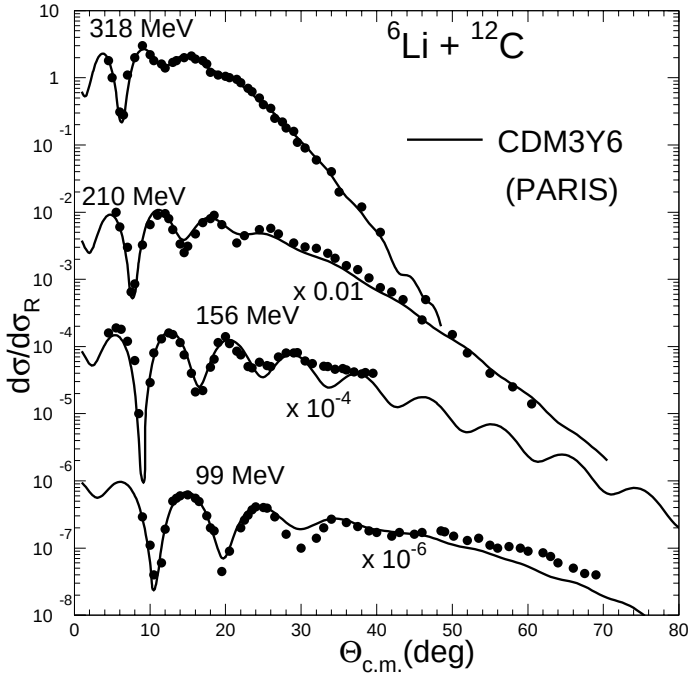

FIG. 13: Elastic scattering data for ^{6}Li + ^{12}C at 99, 156, 210 et 318 MeV in comparison with the results given by the real folded potential. The best-fit renormalization factor N_r of the real folded potential and parameters of the imaginary potential are discussed in the text.

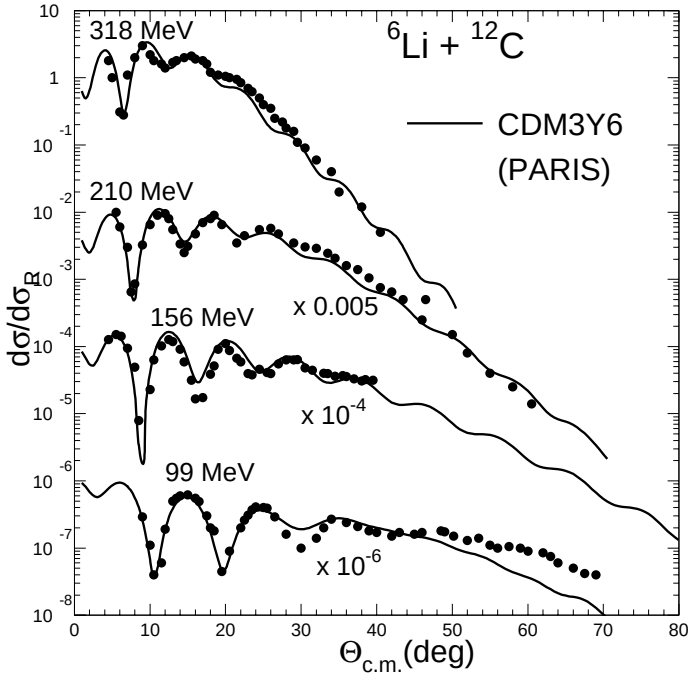

FIG. 14: Elastic scattering data for ^{6}Li + ^{12}C at 99, 156, 210 et 318 MeV in comparison with the results given by the real folded potential. The normalization factor N_r and the diffuseness of the imaginary potential were fixed as $N_r = 0.85$ and $a_w = 0.6$ at 156-318 MeV in the OM search. The parameters are explained in the text and given in Table V.

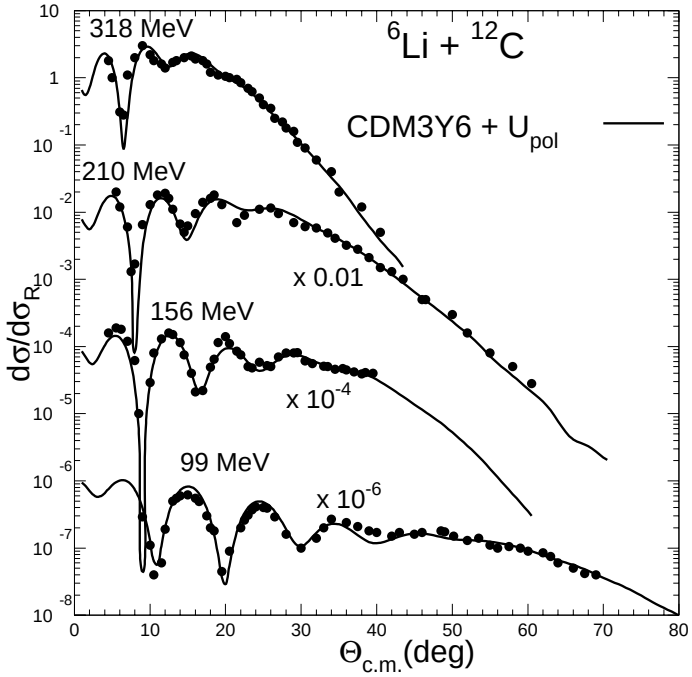

FIG. 15: Elastic scattering data for ^{6}Li + ^{12}C at 99, 156, 210 et 318 MeV are compared with the OM results given by the unrenormalized folded potential added to a polarization potential whose parameters are explained in the text.

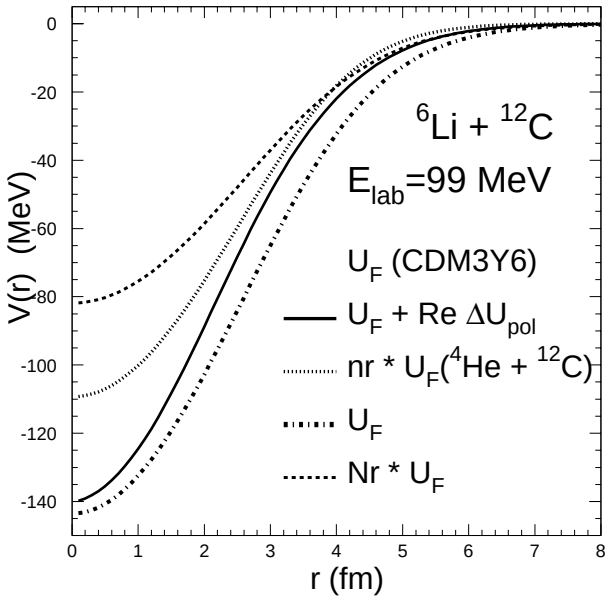

FIG. 16: Real folded potentials calculated with CDM3Y6, for the elastic scattering of ^{6}Li+^{12}C at E_{lab} = 99 MeV (16.5 MeV/nucleon). The unrenormalized folded potential U_F is shown with the dash-dotted line. The renormalized potential with the factor N_r given in Table V is presented by the long-dashed curve. The total potential obtained by adding the polarization potential (parameters are in table VI) to U_F is drawn with the solid curve. For comparison, the CDM3Y6 potential of the ^{4}He+^{12}C system at 16.5 MeV/nucleon (normalized with the factor deduced in section III) is also presented, by the dotted line.

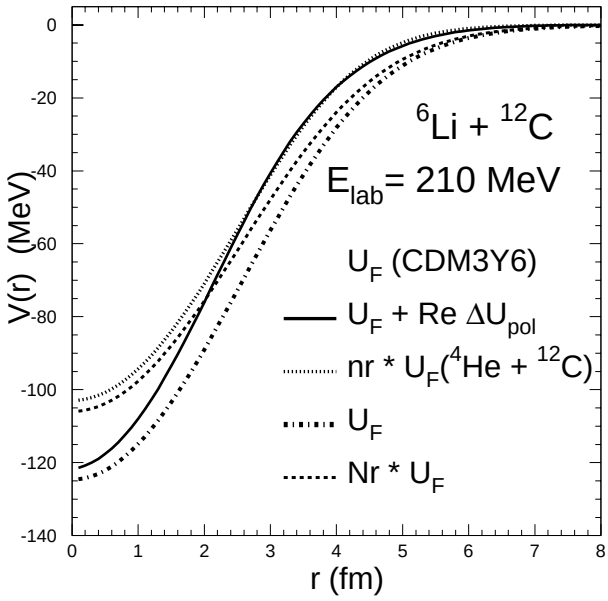

FIG. 17: The same as Fig. 16 but at $E_{lab} = 210$ MeV (35 MeV/nucleon).

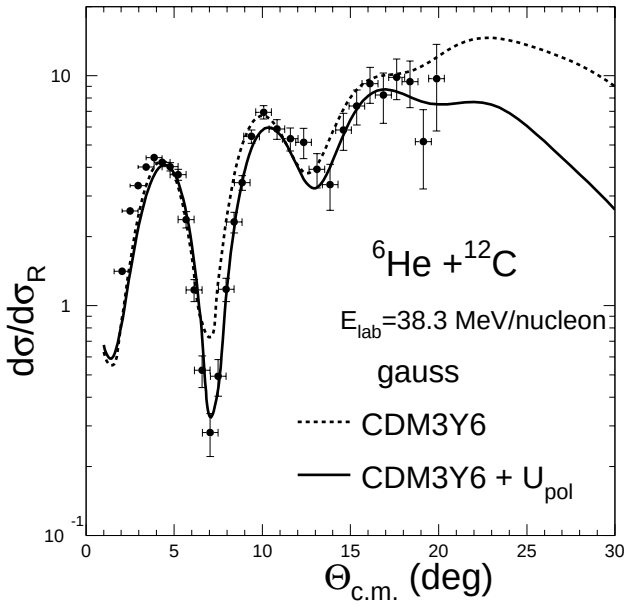

FIG. 18: Elastic scattering for ^{6}He + ^{12}C at 38.3 MeV/nucleon in comparison with the OM results given by the real folded potential and the Gaussian density ga for ^{6}He. The dashed curve is realized with the CDM3Y6 potential alone. The solid curve is obtained by adding a complex surface DPP, with radius R_{pol}, to the optical potential. The parameters for the potentials are explained in the text.

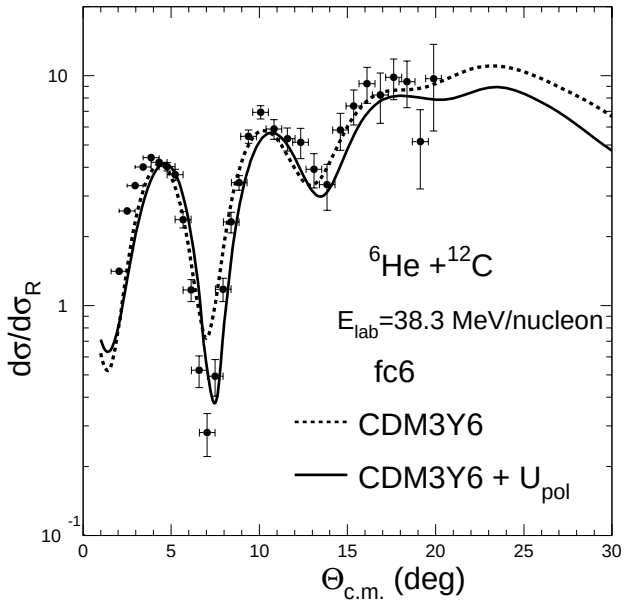

FIG. 19: The same as Fig. 18 but with the *fc6* density and the DPP with parameters given in Table VII.

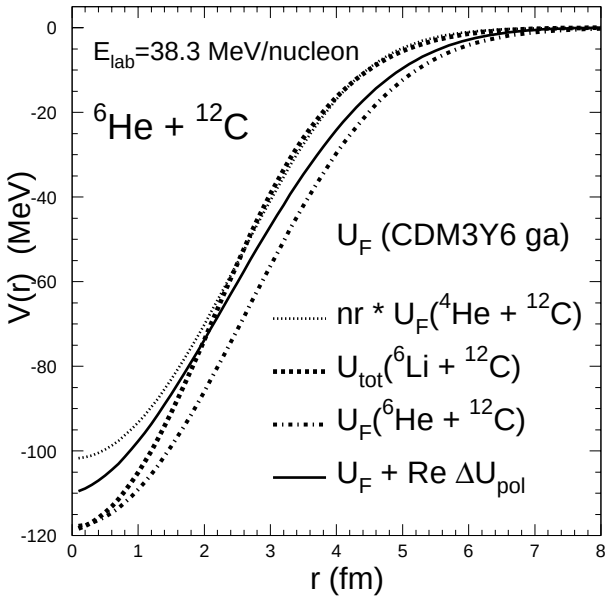

FIG. 20: Real folded potentials calculated with CDM3Y6, for the ^{6}He+^{12}C system at 38.3 MeV/nucleon. The unrenormalized folded potential U_F is shown with the dash-dotted line. The potential corresponding to the ^{6}Li+^{12}C scattering at 38.3 MeV/nucleon, with the parameters given in Table VI is presented by the long-dashed curve. The total potential obtained by adding U_F to the polarization potential (parameters are in table VII) is drawn with the solid curve. For comparison, the CDM3Y6 potential for the ^{4}He+^{12}C system at 38.3 MeV/nucleon (normalized with the factor deduced in section III) is also presented by the dotted line.

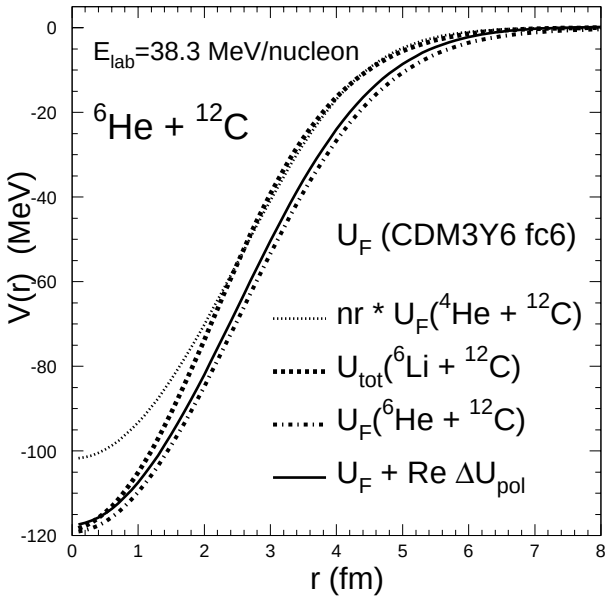

FIG. 21: The same as Fig. 20 but using the *fc6* density.

NN	density	N_r	W_v MeV	R_w (r_w) fm	a_w fm	σ_R (mb)
BDM3Y1	*fc6*	0.9	6.383	6.426 (1.565)	0.378	1172.
CDM3Y6	*ga*	0.95	7.67	6.04 (1.471)	0.524	1179.
CDM3Y6	*fc6*	0.9	6.343	6.445(1.569)	0.358	1169.

TABLE I: Parameters of the optical potential for the ^{6}He $+^{12}$C system at 38.3 MeV/nucleon. The real folded potential for is calculated with the BDM3Y1 or the CDM3Y6 interaction, and with *fc6* or the gaussian one (both have an rms radius equal to 2.54 fm). The normalization factor N_r and the WS imaginary potential are discussed in the text. r_w is the reduced radius of the imaginary part.

Energy MeV/nucleon	E MeV	g(E)	N_r	$J_V/(4A)$ MeV.fm^3	$\langle r^2\rangle_V^{1/2}$ fm	W_v MeV	R_w fm	a_w fm	χ^2/N	σ_R (mb)
26	104	0.9220	1.105	314.2	3.383	23.84	3.39	0.665	6.1	784.7
34.75	139	0.8957	1.213	321.3	3.393	19.98	3.979	0.495	3.6	745.3
43.125	172.5	0.8706	1.098	243.8	3.411	19.92	3.754	0.602	1.9	717.8

TABLE II: Parameters (N_r, W_v, R_w) of the optical potential for the three sets of α + ^{12}C data analyzed in the framework of the folding model, with CDM3Y6.

Energy MeV/nucleon	E MeV	$J_V/(4A)$ MeV.fm^3	$\langle r^2\rangle_V^{1/2}$ fm	W_v MeV	χ^2/N	σ_R (mb)
26	104	331.2	3.383	19.05	7.53	792.0
34.75	139	308.6	3.393	21.4	5.86	766.1
43.125	172.5	258.7	3.411	22.4	4.25	746.9

TABLE III: Same as for table II but with N_r=1.165, R_w=3.76 fm and a_w=0.6 fixed, as described in the text.

Energy MeV/nucleon	E MeV	g(E)	N_r	W_v MeV	R_w (r_w) fm	a_w fm	χ^2/N	σ_R (mb)
16.5	99	0.9505	0.614	195.4	0.29(0.07)	1.31	9.9	1534
26.	156	0.922	0.85	212.	3.37(0.82)	0.560	7.6	1080.
35.	210	0.895	0.854	68.7	3.45(0.939)	0.687	5.1	1023.
53.	318	0.841	0.832	75.0	1.76(0.429)	1.23	1.5	1184.

TABLE IV: Parameters of the optical potential for the ^{6}Li +^{12}C system at 4 energies. The real folded potential is obtained with the CDM3Y6 interaction. r_w is the reduced radius of the WS imaginary potential.

Energy MeV/nucleon	E MeV	g(E)	N_r	W_v MeV	R_w (r_w) fm	a_w fm	χ^2/N	σ_R (mb)
16.5	99	0.9505	0.565	42.6	2.29(0.558)	1.37	13.7	1626.
26.	156	0.922	0.85	94.1	3.696(0.9)	0.6	8.8	1094.
35.	210	0.895	0.85	54.9	3.86(0.939)	0.6	5.7	998.
53.	318	0.841	0.85	37.4	3.99(0.97)	0.6	12.3	904.

TABLE V: The same as in Table IV but with N_r=0.85 and a_w= 0.6 fm fixed in the OM search for the three data sets at high energies.

Energy MeV/nucleon	E MeV	W_v MeV	R_w (r_w) fm	a_w fm	V_{pol} MeV	a_{pol} fm	R_{pol} fm	W_{pol} MeV	χ^2/N	σ_R (mb)
16.5	99	21.86	2.24(0.546)	1.181	−63.9	0.95	2.7	57.44	4.4	1388.
26.	156	20.0	3.983(0.97)	0.751	−48.4	0.95	2.85	23.1	3.1	1146.
35.	210	20.0	3.983(0.97)	0.887	−63.1	0.95	2.85	3.71	6.8	1079.
53.	318	20.0	3.983(0.97)	0.95	−44.4	0.95	2.85	1.03	5.5	1051.

TABLE VI: Parameters of the optical potential for the ^{6}Li+^{12}C system at 4 different energies. The total optical potential includes *unrenormalized* real folded potential, WS imaginary potential and a parametrized polarization potential (13). W_v, R_w, R_{pol}, and a_{pol} were fixed in the OM search for the three data sets at high energies.

Interaction	density	W_v MeV	$R_w(r_w)$ fm	a_w fm	V_{pol} MeV	a_{pol} fm	R_{pol} fm	W_{pol} MeV	σ_R (mb)
CDM3Y6	*ga*	20.0	3.983(0.97)	0.89	-49.2	1.2	1.70	3.2	1092.
CDM3Y6	*fc6*	20.0	3.983(0.97)	0.7	-12.	1.69	2.81	3.2	1058.

TABLE VII: Parameters of the optical potential for the ^{6}He+^{12}C system at 38.3 MeV/nucleon. The real folded potential is obtained with either *fc6* or Gaussian *ga* density for ^{6}He (both have an rms radius equal 2.54 fm). The total optical potential includes *unrenormalized* real folded potential, WS imaginary potential and a parametrized polarization potential (13). The depth $W_v = 20$ MeV and radius $R_w = 3.76$ fm of the WS imaginary potential were fixed at values deduced from the ^{6}Li+^{12}C system.